ACS MATERIALS LETTERS

www.acsmaterialsletters.org

LETTER

Colloidal Quantum Dot Solar Cell Band Alignment using Two-Step Ionic Doping

Koen Bertens,[‡] James Z. Fan,[‡] Margherita Biondi, Armin Sedighian Rasouli, Seungjin Lee, Peicheng Li, Bin Sun, Sjoerd Hoogland, F. Pelayo García de Arquer, Zheng-Hong Lu, and Edward H. Sargent*

Cite This: *ACS Materials Lett.* 2020, 2, 1583–1589

Read Online

ACCESS | Metrics & More | Article Recommendations | Supporting Information

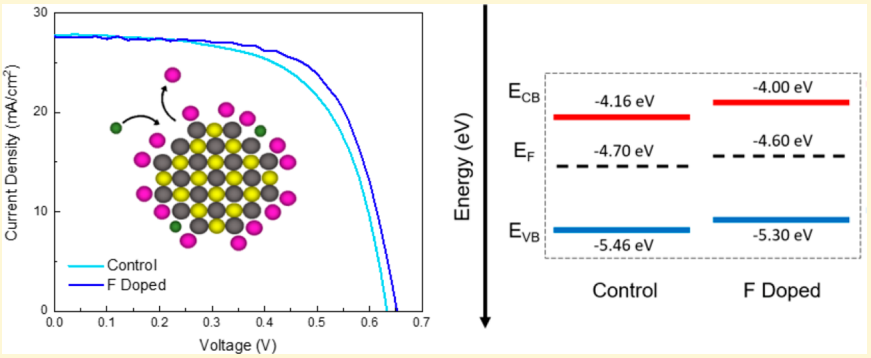

ABSTRACT: **Colloidal quantum dot (CQD) solar cells composed of ionic halide passivated active layers benefit from improved passivation and high carrier mobility because of short interparticle distance. However, non-ideal band alignment of the active layer limits the potential open-circuit voltage (V_{OC}) produced by the solar cell. We initiated a suite of simulation-based studies of CQD solar cells and found a route to improved performance by increasing the degree of p-type behavior. Fluoride, while it is a p-type ionic ligand as desired, is incompatible with traditional ligand exchange processes. In prior studies, it has shown to etch the lead sulfide surface uncontrollably. Instead, we develop a multistep halide exchange method, in which the CQD active layer is doped with fluoride ions after ligand exchange. This new method prevents CQD surface etching without impeding charge transport, resulting in a statistically significant improvement in V_{OC}, fill factor, and power conversion efficiency.**

The quantum confinement effect observed in quantum dots has motivated the rapid progression of recent developments in next-generation optoelectronic devices such as solar cells,[1,2] photodetectors,[3,4] LEDs,[5,6] and lasers.[7,8] The size tunability of these materials allows for selective control of the bandgap by design of reaction conditions, allowing tailoring of the absorption or emission profile.[9] This is especially useful in quantum-dot-based solar cells, where absorption tunability allows solar energy harvesting across the entire AM1.5G spectrum.[10]

Colloidal quantum dot (CQD) devices also greatly benefit from solution processability, enabling deposition of thin films at room temperature using techniques such as spin-coating,[11] blade-coating,[12] and spray deposition.[13] Integral to effective solution processability is the ligand exchange process, where bulky and insulating oleic acid ligands are stripped from the lead sulfide (PbS) CQD surface and replaced with ionic halide ligands, which allow for surface passivation, controlled doping, and closer interparticle packing of CQD films.[14−16] Iodide and bromide anionic ligands are commonly used due to their role in fabricating n-type, air stable, and closely packed CQD films used in photovoltaic devices.[17,18]

Charge collection in CQD solar cells depends on favorable band alignment between the absorbing and transport layers; poor alignment can create potential energy barriers which block electrons or holes from traveling to respective electrodes.[19] Conversely, band alignment exhibiting a large potential energy drop from the active layer to the transport layer can result in electrical power losses.[20] Hence, a close alignment of conduction and valence bands at the interface of the active layer and the transport layer is desired to maximize quasi-Fermi level splitting in the active layer, thereby maximizing

Received: August 14, 2020
Accepted: October 22, 2020
Published: October 30, 2020

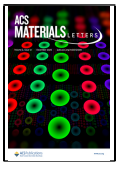

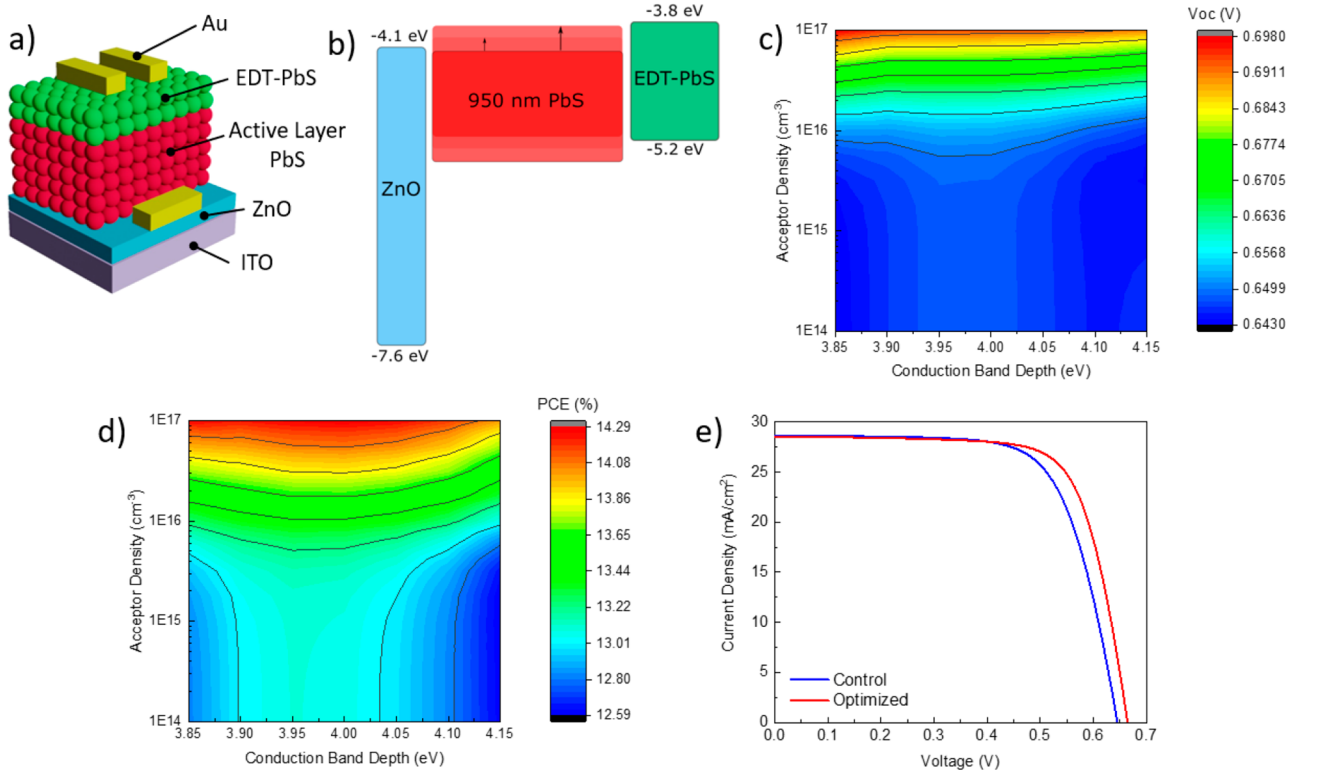

Figure 1. (a) Device schematic of a CQD solar cell based on *n-i-p* architecture; (b) Spatial band alignment scheme of a CQD solar cell showing a variable active layer band alignment; Simulated open-circuit voltage (c) and power conversion efficiency (d) of a CQD solar cell with variable conduction band depth and acceptor density; (e) *J*−*V* curve of an unoptimized and optimized CQD solar cell active layer.

efficiency.[21] Band alignment of the PbS CQD active layer is determined by surface ligand coverage, and many studies have attempted to elucidate the effects of various ligands on the doping profile of the film.[14,22] Of these commonly used ligands, halide anions (I^-, Br^-, Cl^-) exhibit the best n-doping behaviour.[14] They achieve smaller interparticle spacing in assembled thin films than their organic ligand counterparts, allowing for better charge transport and improved device performance.[17] Additionally, I^- passivation prevents oxidation of the PbS surface and enables air stability.[18] Corresponding electron transport layer (ETL) and hole transport layer (HTL) materials are chosen to closely match the conduction and valence bands of the active layer; however, some misalignment still exists between the halide-passivated active layer and the 1,2-ethanedithiol (EDT)-capped PbS HTL, and the full potential of absorbed solar energy is not transformed into electrical power.[23]

When the valence band of the CQD active layer shifts to create closer alignment with the valence band of the EDT-doped HTL, a greater degree of retention of the free energy of carriers across interfaces corresponds to increased open-circuit voltage (V_{OC}).[21] Recent efforts to improve the V_{OC} of CQD solar cells have often targeted the ETL and HTL through doping[24,25] or the interface these layers share with the absorbing CQD active layer.[26] Konstantatos et al. show reductions in V_{OC} losses are accomplished through suppressing carrier recombination in both the bulk[27] and at the interface.[28] Seldom is the doping profile of the active layer targeted; ionic halides provide the shortest interparticle distance and thus the best interdot spacing in CQD films, leaving little freedom to tune the surface ligand composition. While halide ions are known to be n-doping,[18] F^- is comparatively the most p-type, or least n-type, of these ligands. This is due to its relatively large electron affinity, a property which has been found to shift the Fermi level toward the valence band, indicating a more p-type behavior.[14,29] Its use in this role is underexplored, however, as the poor solubility of PbF_2 in N,N-dimethylformamide (DMF) makes it incompatible with the ligand exchange process. Tetrabutylammonium fluoride layer-by-layer (LBL) ligand exchanges have been explored in PbS solar cells; however, the manufacturing disadvantages from the LBL process coupled with low V_{OC} values call for alternative choices for fluoride-based ligands.[30] Using F^- as a counter-dopant to reduce the high degree of n-type doping behaviour seen in I^- and Br^- doped CQDs can allow for greater tunability of the valence band, conduction band, and Fermi level of this material. Loi et al. show that a greater control of in-solution doping allows for device optimization by tuning energy bands and depletion widths, leading to enhanced PCEs.[31,32]

Herein, we explore the effect of p-type doping of the CQD active layer by varying the magnitude of the conduction band depth and relative dopant levels in a simulation of a CQD device. We determine an optimal depth for the valence and conduction bands leading to improved V_{OC}, fill factor (FF), and power conversion efficiency (PCE), which is achieved by shifting toward greater p-type characteristic than current ligand exchange methods can achieve. On the basis of these results, we develop a multistep halide exchange strategy which bypasses the observed limitations of F^- as an ionic ligand in the ligand exchange process, namely poor solubility of lead fluoride in DMF and etching of the PbS surface by F^-. As a result, we show improved V_{OC}, FF, and PCE of our devices over the controls.

https://dx.doi.org/10.1021/acsmaterialslett.0c00379
ACS Materials Lett. 2020, 2, 1583−1589

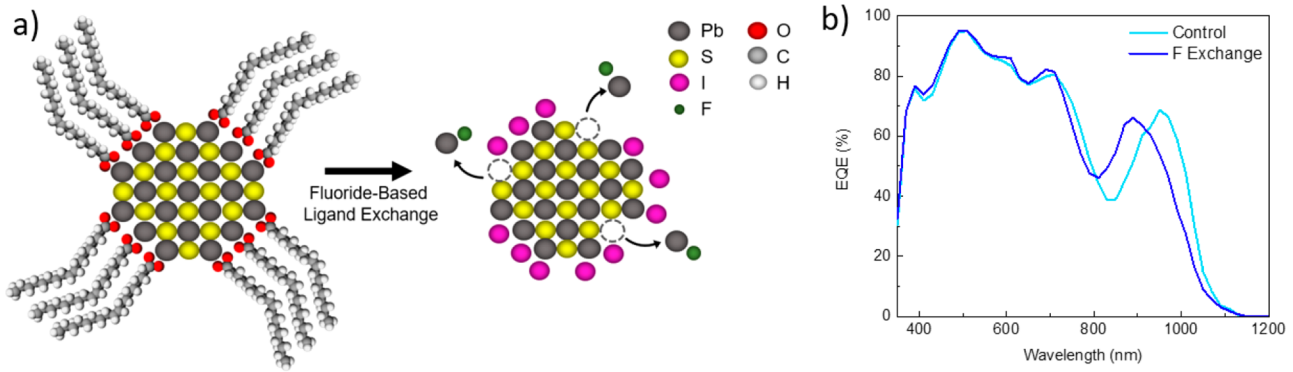

Figure 2. (a) Proposed etching process during fluoride-based ligand exchange in which fluoride ions etch lead from the surface; (b) Measured EQE spectra of CQD solar cells fabricated using non-fluoride and fluoride-based ligand exchanges.

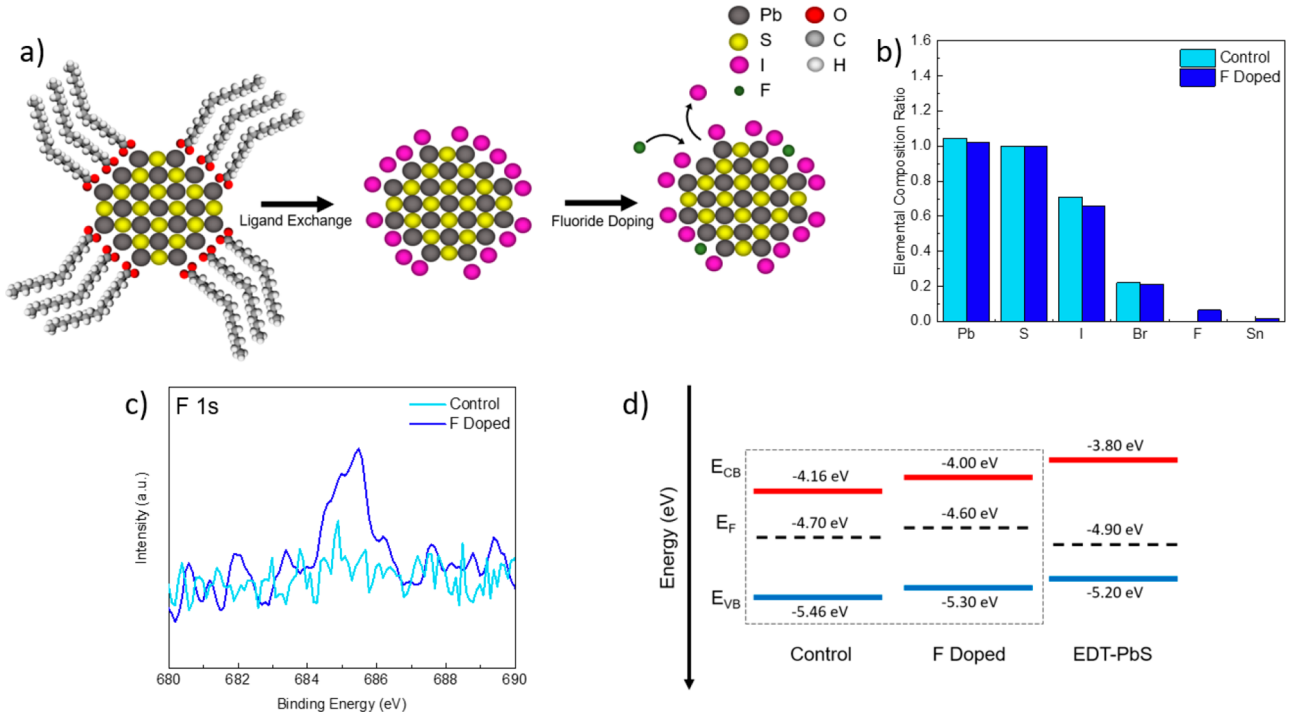

Figure 3. (a) Proposed multistep halide exchange process in which fluoride dopes the CQD surface by displacing halide ligands adsorbed during ligand exchange; (b) XPS elemental composition ratios normalized to sulfur content of the CQDs; (c) XPS spectrum of F 1s; (d) Energy-level diagram of control and fluoride doped CQD films based on UPS data showing valence band, conduction band, and Fermi energy levels compared with those of EDT doped CQD films.

Numerical simulations are of great use to experimental researchers to narrow the direction of their research and preemptively assess the potential success of an experiment. The numerical simulations package SCAPS-1D, a solar cell capacitance simulator,[33] was used to model a planar heterojunction CQD solar cell based on an architecture utilizing zinc oxide (ZnO) as an ETL, EDT-PbS as an HTL, and indium tin oxide (ITO) and gold as electrodes (Figure 1a). We explored the effect of different doping profiles of the active layer by changing the value of the electron affinity and shallow uniform acceptor density of 1.3 eV PbS CQDs, which simulates different degrees of p-type doping causing a Fermi level shift. A range of 3.85 eV to 4.15 eV was chosen to determine an optimal value (Figure 1b), as this range represents typical values for doped CQDs.[14,34,35] We expected that a value too far in either extreme would create band misalignment between either the conduction bands of ZnO and the active layer, or the valence bands of the EDT and active layer, lowering the maximum achievable V_{OC}. The shallow uniform acceptor density was also varied from 10^{14} cm^{-3} to 10^{17} cm^{-3} to simulate the effects of a downshifting Fermi level, which is controlled through the donor to acceptor density ratio in SCAPS. The results (Figure 1c,d) show that both V_{OC} and PCE are improved upon optimization of the doping levels of the active layer, which would normally exhibit a conduction band depth greater than 4.0 eV.[14,23,36] A slight upshift in conduction band height to a value of approximately 3.96 eV promises improvements in V_{OC} and PCE of the device. Similarly, an increase in acceptor density, thus a downshifting of the Fermi level, shows a resulting increase in V_{OC} and PCE as well, though the optimization can be attributed to an overall increase in carrier density at a higher range of concentrations. We compare $J-V$ characteristics (Figure 1e) of a typical control device versus the optimized device exhibiting more p-

https://dx.doi.org/10.1021/acsmaterialslett.0c00379
ACS Materials Lett. 2020, 2, 1583−1589

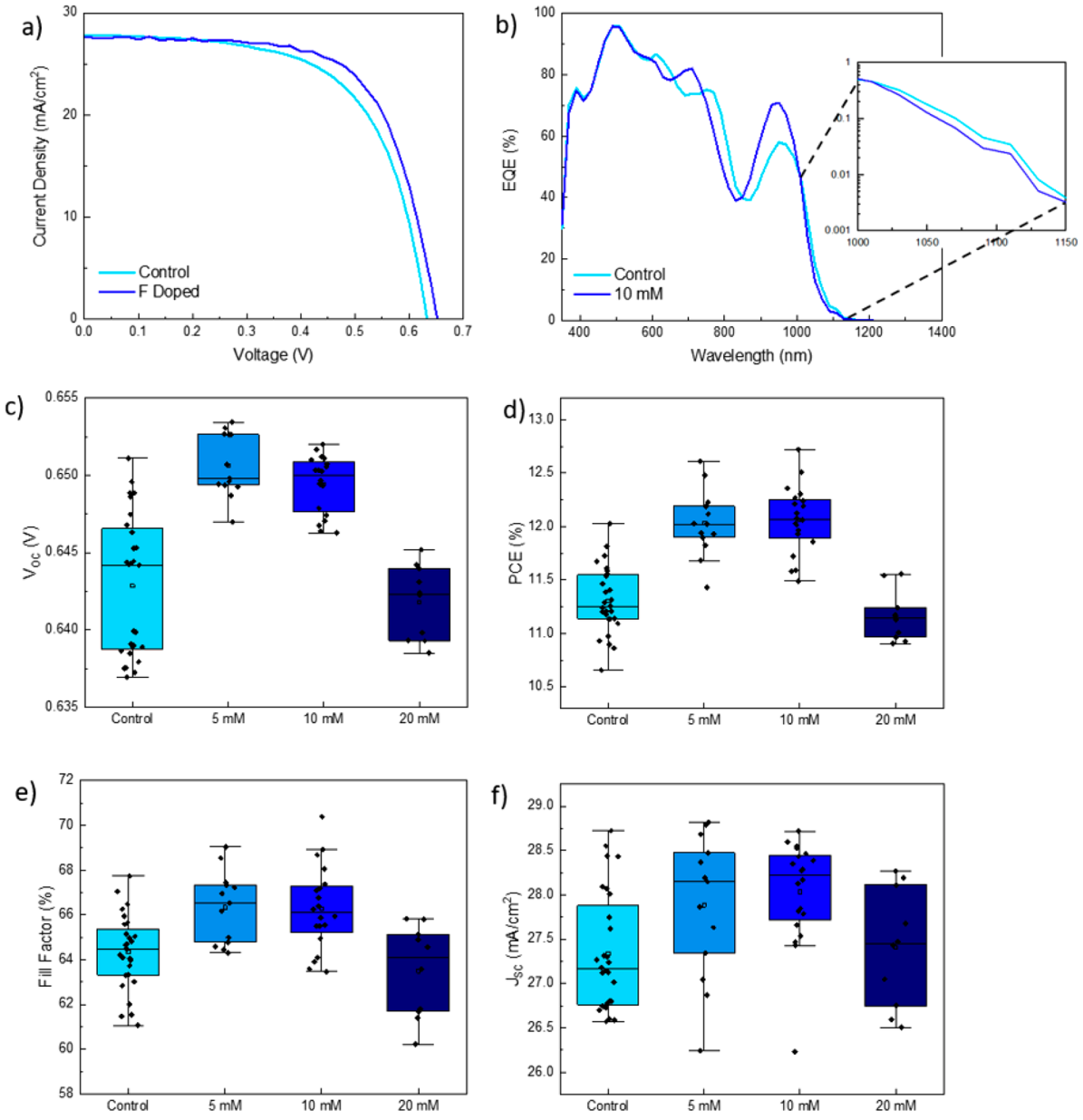

Figure 4. (a) $J-V$ curves of CQD solar cells with control and fluoride-doped active layer; (b) EQE spectra of CQD solar cells with control and fluoride-doped active layer; V_{OC} (c) PCE (d) FF (e) J_{SC} (f) values of CQD solar cells having an active layer doped with 0, 5, 10, and 20 mM fluoride ion matrix.

type doping characteristics, showing an improvement in V_{OC} and FF while J_{SC} remains constant. At higher acceptor concentrations, there occurs a minor decrease in short-circuit current density (J_{SC}) (Supplementary Figure S1a), but this loss is more than counterbalanced by gains in V_{OC} and FF (Supplementary Figure S1b) to result in an increased PCE. Furthermore, we observe a minor improvement in J_{SC} at constant doping levels when the conduction band depth is decreased.

To put theoretical results to practice, a new solution-phase ligand exchange was developed by adding lead fluoride to the existing exchange solution of lead iodide, lead bromide, and ammonium acetate (Figure 2a). The doping effect of fluoride on PbS CQDs has been explored only marginally, but it has shown p-doping characteristic.[14,30] The Pb−F ionic bond is the strongest lead halide bond, and as a result, lead fluoride showed only limited solubility in DMF compared to other lead halides.[37] The addition of a more soluble fluoride species could not solve the solubility issue as fluoride still formed lead fluoride precipitate from lead iodide and lead bromide. A ligand exchange was performed after filtering the new exchange solution containing trace ionic fluoride; however, the resulting devices fabricated using the exchanged CQDs exhibited blue shifting in the excitonic peak of the external quantum efficiency (EQE) measurement by approximately 60 nm (Figure 2b). This was attributed to the etching of lead atoms on the CQD surface by fluoride ions leading to dot shrinkage, which limited the charge collection of the device. The resulting devices also showed a decrease in FF compared with controls which lowered PCE by over 1% (Table S1).

A new strategy was created to circumvent both precipitation of lead fluoride out of the exchange solution and etching of CQDs during ligand exchange, by introducing fluoride ions post-ligand exchange through the addition of a fluoride ion

https://dx.doi.org/10.1021/acsmaterialslett.0c00379
ACS Materials Lett. 2020, 2, 1583−1589

matrix. Tin(II) fluoride, unlike lead fluoride, is sufficiently soluble in DMF and allows for delivery of fluoride ions to the ligand exchanged CQD surface (Figure 3a). Solutions of 5, 10, and 20 mM SnF_2 were added to the final CQD ink dispersions to achieve p-doping. X-ray photoelectron spectroscopy (XPS) (Figure 3b) shows a reduced iodide to sulfur and bromide to sulfur ratio from the control sample to the fluoride doped sample, suggesting that some iodide and bromide ligands are replaced on the surface by fluoride ions. The existing halide ligand coverage protects the underlying lead sulfur surface, preventing etching by fluoride as observed when it is present in the exchange process. A peak at 685 eV in the F 1s XPS spectrum (Figure 3c) of the doped sample confirms the presence of fluoride on the CQD surface, while the peak is absent in the spectrum of the control sample. Surveying the XPS spectra of S 2p and Pb 4f (Supplementary Figure S2a,b), we observe no noticeable shift in the peaks of the spectrum between control sample and fluoride doped sample, indicating a consistency in the oxidation states of the CQD surface upon ligand binding. The valence band and Fermi level energies were investigated using ultraviolet photoelectron spectroscopy (UPS). CQDs having a bandgap of 1.3 eV were measured with and without fluoride matrix doping, and the Fermi level and valence band maximum were determined from the cut-off region and valence band region (Supplementary Figure S3a,b). There is an upward shift in Fermi level energy from −4.7 eV for the undoped CQD film to −4.6 eV for the fluoride doped CQD film. The valence band region of the UPS spectrum shows a similar change in the distance from the Fermi level to the valence band maximum, shifting from 0.76 eV for the undoped film to 0.70 eV for the doped film. Based on a bandgap of 1.3 eV determined by optical absorption, this places the conduction band height of the undoped film at a depth of −4.16 eV, whereas that of the fluoride doped film shifts upward to −4.00 eV, a significantly closer value to the previously determined optimum value of −3.96 eV (Figure 3d).

To further assess the potential success of a fluoride doping strategy, devices were fabricated on a transparent conductive oxide using ITO/ZnO/lead halide-PbS/EDT-PbS/Au planar *n-i-p* architecture, tested under AM1.5G illumination to obtain *J*−*V* characteristics (Figure 4a). Active layers were based on a mixed lead iodide and lead bromide ligand exchange; samples were prepared from CQD ink dispersions with no fluoride doping, 10% added 5 mM fluoride matrix, 10% added 10 mM fluoride matrix, and 10% added 20 mM fluoride matrix (Table S2). The 10 mM sample showed the greatest improvement in PCE over the control, achieving a champion device performance of 12.7%, compared to a champion PCE of 12.0% for the control device. The EQE spectrum (Figure 4b) of the 10 mM fluoride matrix sample showed an improved excitonic peak over the control sample. A logarithmic plot of the band tail absorption showed no considerable difference between the samples, indicating no etching occurred during fluoride doping. Taking in consideration broader trends in the samples, *J*−*V* measurements show an upward statistical trend in the V_{OC} of the devices (Figure 4c), with the middle two quartiles of the 5 mM fluoride-doped CQD devices showing the best improvement. There is a slight decrease in the performance of the middle two quartiles of the 10 mM doped samples, followed by a worsening in V_{OC} at an increased concentration of 20 mM fluoride doping. This trend is similarly reflected in the PCE of the fabricated devices (Figure 4d), which shows a slight improvement in the PCE of the 10 mM fluoride doped samples over that of the 5 mM doped samples, both of which exhibit a clear improvement over the control and 20 mM doped samples. Reflecting on the SCAPS simulation results discussed above, this experimentally observed trend is in agreement with simulated device results. The worse performance of the 20 mM doped devices is ascribed to an overshooting in the conduction band shift above the optimal value of −3.96 eV. An analysis of FF of tested devices (Figure 4e) shows further agreement with simulated results, as again there is a general upward trend from control to moderately fluoride doped CQDs, followed by a drop-off in performance for the most highly doped devices. The improvement in FF is attributed to the optimized alignment between the active layer and HTL, as misalignment of this interface can lead to increased interfacial recombination.[38] Finally, there is a minor upward trend seen in the J_{SC} (Figure 4d) of the samples, which agrees with the simulation data (Supplementary Figure S1a). Based on this data, a fluoride doping concentration of 5 to 10 mM is the optimum to achieve improved device performance through band alignment tuning.

To conclude, we developed a method of doping CQDs with fluoride ion ligands to increase performance. We found that SCAPS provided an effective platform to optimize the performance of a CQD solar cell prior to experimental work. To implement these findings, fluoride was hypothesized to act as an effective p-type ionic ligand. Attaching this ligand via traditional ligand exchange was found to be ineffective, so a post-ligand exchange doping strategy was developed to attach it to the surface instead. Devices made with this method showed statistical improvements in V_{OC}, FF, and PCE, agreeing with the initial simulated results.

■ ASSOCIATED CONTENT

Supporting Information

The Supporting Information is available free of charge at https://pubs.acs.org/doi/10.1021/acsmaterialslett.0c00379.

Experimental methods, SCAPS simulation results, XPS data, UPS data, device performance data, SCAPS parameters (PDF)

■ AUTHOR INFORMATION

Corresponding Author

Edward H. Sargent − *The Edward S. Rogers Department of Electrical and Computer Engineering, University of Toronto, Toronto, Ontario M5S 3G4, Canada;* orcid.org/0000-0003-0396-6495; Email: ted.sargent@utoronto.ca

Authors

Koen Bertens − *The Edward S. Rogers Department of Electrical and Computer Engineering, University of Toronto, Toronto, Ontario M5S 3G4, Canada;* orcid.org/0000-0002-2701-1397

James Z. Fan − *The Edward S. Rogers Department of Electrical and Computer Engineering, University of Toronto, Toronto, Ontario M5S 3G4, Canada;* orcid.org/0000-0002-1594-865X

Margherita Biondi − *The Edward S. Rogers Department of Electrical and Computer Engineering, University of Toronto, Toronto, Ontario M5S 3G4, Canada*

Armin Sedighian Rasouli − *The Edward S. Rogers Department of Electrical and Computer Engineering, University of Toronto,*

https://dx.doi.org/10.1021/acsmaterialslett.0c00379
ACS Materials Lett. 2020, 2, 1583−1589

Toronto, Ontario M5S 3G4, Canada; orcid.org/0000-0002-0807-9468

Seungjin Lee − *The Edward S. Rogers Department of Electrical and Computer Engineering, University of Toronto, Toronto, Ontario M5S 3G4, Canada;* orcid.org/0000-0002-6318-0702

Peicheng Li − *Department of Materials Science and Engineering, University of Toronto, Toronto, Ontario M5S 3E4, Canada*

Bin Sun − *The Edward S. Rogers Department of Electrical and Computer Engineering, University of Toronto, Toronto, Ontario M5S 3G4, Canada;* orcid.org/0000-0002-8233-0999

Sjoerd Hoogland − *The Edward S. Rogers Department of Electrical and Computer Engineering, University of Toronto, Toronto, Ontario M5S 3G4, Canada;* orcid.org/0000-0002-3099-585X

F. Pelayo García de Arquer − *The Edward S. Rogers Department of Electrical and Computer Engineering, University of Toronto, Toronto, Ontario M5S 3G4, Canada;* orcid.org/0000-0003-2422-6234

Zheng-Hong Lu − *Department of Materials Science and Engineering, University of Toronto, Toronto, Ontario M5S 3E4, Canada;* orcid.org/0000-0003-2050-0822

Complete contact information is available at: https://pubs.acs.org/10.1021/acsmaterialslett.0c00379

Author Contributions

‡K.B. and J.Z.F. contributed equally.

Funding

This research was funded by the Ontario Research Fund-Research Excellence program (ORF7-Ministry of Research and Innovation, Ontario Research Fund Research Excellence Round 7), the Natural Sciences and Engineering Research Council of Canada (NSERC), and the Queen Elizabeth II Graduate Scholarship in Science & Technology. The authors acknowledge the financial support from QD Solar Inc.

Notes

The authors declare no competing financial interest.

■ ACKNOWLEDGMENTS

The authors thank L. Levina, E. Palmiano, R. Wolowiec, and D. Kopilovic for their assistance during the period of study.

■ ABBREVIATIONS

CQD, colloidal quantum dot; V_{OC}, open-circuit voltage; ETL, electron transport layer; HTL, hole transport layer; EDT, 1,2-ethanedithiol; DMF, *N*,*N*-dimethylformamide; LBL, layer-by-layer; PCE, power conversion efficiency; ITO, indium tin oxide; J_{SC}, short-circuit current; FF, fill factor; EQE, external quantum efficiency; XPS, X-ray photoelectron spectroscopy; UPS, ultraviolet photoelectron spectroscopy

■ REFERENCES

(1) Emin, S.; Singh, S. P.; Han, L.; Satoh, N.; Islam, A. Colloidal Quantum Dot Solar Cells. *Sol. Energy* **2011**, *85*, 1264−1282.

(2) Luther, J. M.; Law, M.; Beard, M. C.; Song, Q.; Reese, M. O.; Ellingson, R. J.; Nozik, A. J. Schottky Solar Cells Based on Colloidal Nanocrystal Films. *Nano Lett.* **2008**, *8*, 3488−3492.

(3) Ackerman, M. M.; Tang, X.; Guyot-Sionnest, P. Fast and Sensitive Colloidal Quantum Dot Mid-Wave Infrared Photodetectors. *ACS Nano* **2018**, *12*, 7264−7271.

(4) Livache, C.; Martinez, B.; Goubet, N.; Gréboval, C.; Qu, J.; Chu, A.; Royer, S.; Ithurria, S.; Silly, M. G.; Dubertret, B.; Lhuillier, E. A Colloidal Quantum Dot Infrared Photodetector and Its Use for Intraband Detection. *Nat. Commun.* **2019**, *10*, 1−10.

(5) Caruge, J. M.; Halpert, J. E.; Wood, V.; Bulovíc, V.; Bawendi, M. G. Colloidal Quantum-Dot Light-Emitting Diodes with Metal-Oxide Charge Transport Layers. *Nat. Photonics* **2008**, *2*, 247−250.

(6) Park, M.; Song, J.; An, M.; Lim, J.; Lee, C.; Roh, J.; Lee, D. Colloidal Quantum Dot Light-Emitting Diodes Employing Solution-Processable Tin Dioxide Nanoparticles in an Electron Transport Layer. *RSC Adv.* **2020**, *10*, 8261−8265.

(7) Geiregat, P.; Van Thourhout, D.; Hens, Z. A Bright Future for Colloidal Quantum Dot Lasers. *NPG Asia Mater.* **2019**, *11*, 41.

(8) Dang, C.; Lee, J.; Breen, C.; Steckel, J. S.; Coe-Sullivan, S.; Nurmikko, A. Red, Green and Blue Lasing Enabled by Single-Exciton Gain in Colloidal Quantum Dot Films. *Nat. Nanotechnol.* **2012**, *7*, 335−339.

(9) Epps, R. W.; Bowen, M. S.; Volk, A. A.; Abdel-Latif, K.; Han, S.; Reyes, K. G.; Amassian, A.; Abolhasani, M. Artificial Chemist: An Autonomous Quantum Dot Synthesis Bot. *Adv. Mater.* **2020**, *32*, 2001626.

(10) Wang, H.; Kubo, T.; Nakazaki, J.; Segawa, H. Solution-Processed Short-Wave Infrared PbS Colloidal Quantum Dot/ZnO Nanowire Solar Cells Giving High Open-Circuit Voltage. *ACS Energy Lett.* **2017**, *2*, 2110−2117.

(11) Zhang, Z.; Shi, C.; Chen, J.; Xiao, G.; Li, L. Combination of Short-Length TiO 2 Nanorod Arrays and Compact PbS Quantum-Dot Thin Films for Efficient Solid-State Quantum-Dot-Sensitized Solar Cells. *Appl. Surf. Sci.* **2017**, *410*, 8−13.

(12) Kirmani, A. R.; Sheikh, A. D.; Niazi, M. R.; Haque, M. A.; Liu, M.; de Arquer, F. P. G.; Xu, J.; Sun, B.; Voznyy, O.; Gasparini, N.; Baran, D.; Wu, T.; Sargent, E. H.; Amassian, A. Solar Cells: Overcoming the Ambient Manufacturability-Scalability-Performance Bottleneck in Colloidal Quantum Dot Photovoltaics (Adv. Mater. 35/2018). *Adv. Mater.* **2018**, *30*, 1870260.

(13) Choi, H.; Lee, J. G.; Mai, X. D.; Beard, M. C.; Yoon, S. S.; Jeong, S. Supersonically Spray-Coated Colloidal Quantum Dot Ink Solar Cells. *Sci. Rep.* **2017**, *7*, 1−8.

(14) Brown, P. R.; Kim, D.; Lunt, R. R.; Zhao, N.; Bawendi, M. G.; Grossman, J. C.; Bulović, V. Energy Level Modification in Lead Sulfide Quantum Dot Thin Films through Ligand Exchange. *ACS Nano* **2014**, *8*, 5863−5872.

(15) Tang, J.; Kemp, K. W.; Hoogland, S.; Jeong, K. S.; Liu, H.; Levina, L.; Furukawa, M.; Wang, X.; Debnath, R.; Cha, D.; Chou, K. W.; Fischer, A.; Amassian, A.; Asbury, J. B.; Sargent, E. H. Colloidal-Quantum-Dot Photovoltaics Using Atomic-Ligand Passivation. *Nat. Mater.* **2011**, *10*, 765−771.

(16) Chuang, C. H. M.; Brown, P. R.; Bulović, V.; Bawendi, M. G. Improved Performance and Stability in Quantum Dot Solar Cells through Band Alignment Engineering. *Nat. Mater.* **2014**, *13*, 796−801.

(17) Liu, M.; Voznyy, O.; Sabatini, R.; García De Arquer, F. P.; Munir, R.; Balawi, A. H.; Lan, X.; Fan, F.; Walters, G.; Kirmani, A. R.; Hoogland, S.; Laquai, F.; Amassian, A.; Sargent, E. H. Hybrid Organic-Inorganic Inks Flatten the Energy Landscape in Colloidal Quantum Dot Solids. *Nat. Mater.* **2017**, *16*, 258−263.

(18) Ning, Z.; Voznyy, O.; Pan, J.; Hoogland, S.; Adinolfi, V.; Xu, J.; Li, M.; Kirmani, A. R.; Sun, J. P.; Minor, J.; Kemp, K. W.; Dong, H.; Rollny, L.; Labelle, A.; Carey, G.; Sutherland, B.; Hill, I.; Amassian, A.; Liu, H.; Tang, J.; Bakr, O. M.; Sargent, E. H. Air-Stable n-Type Colloidal Quantum Dot Solids. *Nat. Mater.* **2014**, *13*, 822−828.

(19) Lee, S.; Zhitomirsky, D.; Grossman, J. C. Manipulating Electronic Energy Disorder in Colloidal Quantum Dot Solids for Enhanced Charge Carrier Transport. *Adv. Funct. Mater.* **2016**, *26*, 1554−1562.

(20) Lim, K. G.; Ahn, S.; Kim, Y. H.; Qi, Y.; Lee, T. W. Universal Energy Level Tailoring of Self-Organized Hole Extraction Layers in Organic Solar Cells and Organic-Inorganic Hybrid Perovskite Solar Cells. *Energy Environ. Sci.* **2016**, *9*, 932−939.

(21) Stolterfoht, M.; Caprioglio, P.; Wolff, C. M.; Márquez, J. A.; Nordmann, J.; Zhang, S.; Rothhardt, D.; Hörmann, U.; Amir, Y.;

Redinger, A.; Kegelmann, L.; Zu, F.; Albrecht, S.; Koch, N.; Kirchartz, T.; Saliba, M.; Unold, T.; Neher, D. The Impact of Energy Alignment and Interfacial Recombination on the Internal and External Open-Circuit Voltage of Perovskite Solar Cells. *Energy Environ. Sci.* **2019**, *12*, 2778−2788.

(22) Santra, P. K.; Palmstrom, A. F.; Tanskanen, J. T.; Yang, N.; Bent, S. F. Improving Performance in Colloidal Quantum Dot Solar Cells by Tuning Band Alignment through Surface Dipole Moments. *J. Phys. Chem. C* **2015**, *119*, 2996−3005.

(23) Biondi, M.; Choi, M. J.; Ouellette, O.; Baek, S. W.; Todorović, P.; Sun, B.; Lee, S.; Wei, M.; Li, P.; Kirmani, A. R.; Sagar, L. K.; Richter, L. J.; Hoogland, S.; Lu, Z. H.; García de Arquer, F. P.; Sargent, E. H. A Chemically Orthogonal Hole Transport Layer for Efficient Colloidal Quantum Dot Solar Cells. *Adv. Mater.* **2020**, *32*, 1906199.

(24) Wang, L.; Jia, Y.; Wang, Y.; Zang, S.; Wei, S.; Li, J.; Zhang, X. Defect Passivation of Low-Temperature Processed ZnO Electron Transport Layer with Polyethylenimine for PbS Quantum Dot Photovoltaics. *ACS Appl. Energy Mater.* **2019**, *2*, 1695−1701.

(25) Teh, Z. L.; Hu, L.; Zhang, Z.; Gentle, A. R.; Chen, Z.; Gao, Y.; Yuan, L.; Hu, Y.; Wu, T.; Patterson, R. J.; Huang, S. Enhanced Power Conversion Efficiency via Hybrid Ligand Exchange Treatment of P-Type PbS Quantum Dots. *ACS Appl. Mater. Interfaces* **2020**, *12*, 22751−22759.

(26) Hong, J.; Kim, B. S.; Hou, B.; Cho, Y.; Lee, S. H.; Pak, S.; Morris, S. M.; Sohn, J. I.; Cha, S. N. Plasmonic Effects of Dual-Metal Nanoparticle Layers for High-Performance Quantum Dot Solar Cells. *Plasmonics* **2020**, *15*, 1007−1013.

(27) Pradhan, S.; Stavrinadis, A.; Gupta, S.; Christodoulou, S.; Konstantatos, G. Breaking the Open-Circuit Voltage Deficit Floor in PbS Quantum Dot Solar Cells through Synergistic Ligand and Architecture Engineering. *ACS Energy Lett.* **2017**, *2*, 1444−1449.

(28) Pradhan, S.; Stavrinadis, A.; Gupta, S.; Konstantatos, G. Reducing Interface Recombination through Mixed Nanocrystal Interlayers in PbS Quantum Dot Solar Cells. *ACS Appl. Mater. Interfaces* **2017**, *9*, 27390−27395.

(29) Kirmani, A. R.; Kiani, A.; Said, M. M.; Voznyy, O.; Wehbe, N.; Walters, G.; Barlow, S.; Sargent, E. H.; Marder, S. R.; Amassian, A. Remote Molecular Doping of Colloidal Quantum Dot Photovoltaics. *ACS Energy Lett.* **2016**, *1*, 922−930.

(30) Bederak, D.; Balazs, D. M.; Sukharevska, N. V.; Shulga, A. G.; Abdu-Aguye, M.; Dirin, D. N.; Kovalenko, M. V.; Loi, M. A. Comparing Halide Ligands in PbS Colloidal Quantum Dots for Field-Effect Transistors and Solar Cells. *ACS Appl. Nano Mater.* **2018**, *1*, 6882−6889.

(31) Speirs, M. J.; Dirin, D. N.; Abdu-Aguye, M.; Balazs, D. M.; Kovalenko, M. V.; Loi, M. A. Temperature Dependent Behaviour of Lead Sulfide Quantum Dot Solar Cells and Films. *Energy Environ. Sci.* **2016**, *9*, 2916−2924.

(32) Speirs, M. J.; Balazs, D. M.; Dirin, D. N.; Kovalenko, M. V.; Loi, M. A. Increased Efficiency in Pn-Junction PbS QD Solar Cells via NaHS Treatment of the p-Type Layer. *Appl. Phys. Lett.* **2017**, *110*, 103904.

(33) Burgelman, M.; Nollet, P.; Degrave, S. Modelling Polycrystalline Semiconductor Solar Cells. *Thin Solid Films* **2000**, *361*, 527−532.

(34) Choi, M. J.; Oh, J.; Yoo, J. K.; Choi, J.; Sim, D. M.; Jung, Y. S. Tailoring of the PbS/Metal Interface in Colloidal Quantum Dot Solar Cells for Improvements of Performance and Air Stability. *Energy Environ. Sci.* **2014**, *7*, 3052−3060.

(35) Stavrinadis, A.; Pradhan, S.; Papagiorgis, P.; Itskos, G.; Konstantatos, G. Suppressing Deep Traps in PbS Colloidal Quantum Dots via Facile Iodide Substitutional Doping for Solar Cells with Efficiency >10%. *ACS Energy Lett.* **2017**, *2*, 739−744.

(36) Choi, M. J.; García de Arquer, F. P.; Proppe, A. H.; Seifitokaldani, A.; Choi, J.; Kim, J.; Baek, S. W.; Liu, M.; Sun, B.; Biondi, M.; Scheffel, B.; Walters, G.; Nam, D. H.; Jo, J. W.; Ouellette, O.; Voznyy, O.; Hoogland, S.; Kelley, S. O.; Jung, Y. S.; Sargent, E. H. Cascade Surface Modification of Colloidal Quantum Dot Inks Enables Efficient Bulk Homojunction Photovoltaics. *Nat. Commun.* **2020**, *11*, 1−9.

(37) Li, N.; Tao, S.; Chen, Y.; Niu, X.; Onwudinanti, C. K.; Hu, C.; Qiu, Z.; Xu, Z.; Zheng, G.; Wang, L.; Zhang, Y.; Li, L.; Liu, H.; Lun, Y.; Hong, J.; Wang, X.; Liu, Y.; Xie, H.; Gao, Y.; Bai, Y.; Yang, S.; Brocks, G.; Chen, Q.; Zhou, H. Cation and Anion Immobilization through Chemical Bonding Enhancement with Fluorides for Stable Halide Perovskite Solar Cells. *Nat. Energy* **2019**, *4*, 408−415.

(38) Sharbati, S.; Sites, J. R. Impact of the Band Offset for N-Zn(O,S)/p-Cu(In,Ga)Se2 Solar Cells. *IEEE J. Photovoltaics* **2014**, *4*, 697−702.

https://dx.doi.org/10.1021/acsmaterialslett.0c00379
ACS Materials Lett. 2020, 2, 1583−1589